


## Article

# Numerical Study on the Cavitation Flow and Its Effect on the Structural Integrity of Multi-Stage Orifice

Gonghee Lee <sup>1,\*</sup> , Myungjo Jung <sup>2</sup>, Juneho Bae <sup>1</sup> and Soonho Kang <sup>3</sup>

<sup>1</sup> Department of Regulatory Assessment, Korea Institute of Nuclear Safety, Daejeon 34142, Korea; bum5520@kins.re.kr

<sup>2</sup> Department of Nuclear Safety Research, Korea Institute of Nuclear Safety, Daejeon 34142, Korea; mjj@kins.re.kr

<sup>3</sup> Department of Kori NPP Regulation, Korea Institute of Nuclear Safety, Daejeon 34142, Korea; k728ksh@kins.re.kr

\* Correspondence: ghlee@kins.re.kr; Tel.: +82-42-868-0683

**Abstract:** Flow leakage due to cavitation erosion occurred at the socket welding part downstream of the multi-stage orifice installed in the auxiliary feedwater (AFW) pump recirculation line of the domestic nuclear power plant (NPP). To assess the adequacy of the changed operating flow rate proposed by a domestic NPP operator as the corrective measure concerning the flow leakage in the AFW pump recirculation line, the pattern of the cavitation flow in the eight-stage orifice and the connecting pipe depending on the magnitude of the operating flow rate was predicted by using ANSYS CFX R19.1. Additionally, using ANSYS Mechanical, the structural analysis was conducted under the same operating flow rate condition used for the flow analysis, and the structural integrity was evaluated for the allowable stress. Based on the flow analysis results, it was found that the operating flow rate was the main factor to influence the cavitation behavior inside the multi-stage orifice, and cavitation flow still happened even in the vicinity of the corrected operating flow rate, so it should be necessary to fundamentally review the adequacy of the multi-stage orifice design. On the other hand, the geometric dimensions and arrangement of orifice hole position at the individual stage of the multi-stage orifice may have a significant influence on the characteristics of pressure drop and flow patterns (including cavitation). Therefore, these effects were examined by simulating an analysis model in which the hole diameter of the eighth-stage orifice was changed under the design flow rate condition. As a result of flow analysis, it was found that reducing the hole diameter in the eighth stage orifice resulted in increasing the pressure drop. In relation to the structural integrity of the eight-stage orifice and the connecting pipe, it was found that its integrity could be maintained under the design and operating flow rate conditions.

**Keywords:** auxiliary feedwater system; cavitation; computational fluid dynamics; in-service testing; multiphase flow; multi-stage orifice



**Citation:** Lee, G.; Jung, M.; Bae, J.; Kang, S. Numerical Study on the Cavitation Flow and Its Effect on the Structural Integrity of Multi-Stage Orifice. *Energies* **2021**, *14*, 1518. <https://doi.org/10.3390/en14061518>

Academic Editor:  
Pouyan Talebizadeh Sardari

Received: 29 December 2020  
Accepted: 6 March 2021  
Published: 10 March 2021

**Publisher's Note:** MDPI stays neutral with regard to jurisdictional claims in published maps and institutional affiliations.



**Copyright:** © 2021 by the authors. Licensee MDPI, Basel, Switzerland. This article is an open access article distributed under the terms and conditions of the Creative Commons Attribution (CC BY) license (<https://creativecommons.org/licenses/by/4.0/>).

## 1. Introduction

Nuclear power plant (NPP) operators periodically conduct in-service testing (IST) for pumps that perform safety functions and monitor/evaluate the degree of their vulnerability over time. The auxiliary feedwater (AFW) system, one of the representative IST-related systems, plays a role in supplying the coolant to remove heat from the primary system when the main feedwater (MFW) system cannot be used in an emergency, including a small break loss-of-coolant-accident. As shown in Figure 1, this system consists of the main flow line for injecting coolant from the AFW pump to the steam generator and a recirculation line for the safe operation and performance tests of the AFW pump. The multi-stage orifice is installed in the recirculation line to limit the flow rate at the high discharge pressure of the AFW pump and perform the system decompression function.

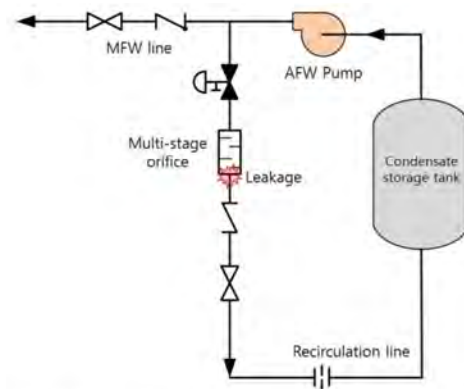


**Figure 1.** Schematic diagram for the auxiliary feedwater (AFW) pump recirculation line of the domestic nuclear power plant (NPP).

As shown in Figure 2, in the domestic NPP, while the reactor coolant system maintained the normal operating temperature/pressure and the motor-driven AFW pump supplied the coolant to the steam generator, flow leakage occurred at the socket welding part downstream of the multi-stage orifice. As a result of analyzing the pipe specimen with an optical microscope, the domestic NPP operator deduced that the pipe wall thinning occurred due to erosion, forming a rough surface, and the thinning passed through the pipe and proceeded to the welding part [1]. In conclusion, the cavitation erosion due to the bubbles collapse was suggested as the main cause of the flow leakage at the welding part [1].

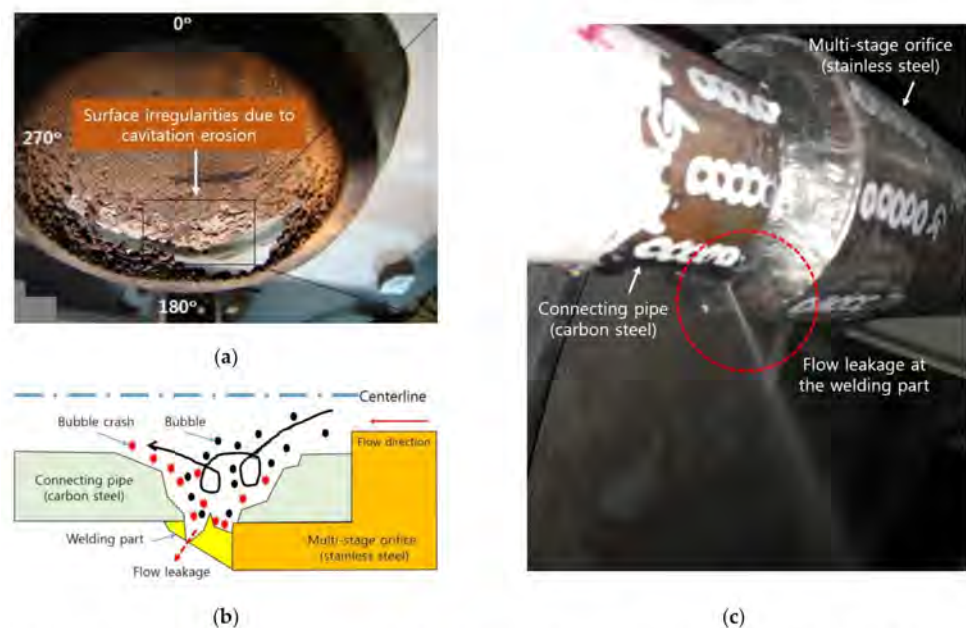


**Figure 2.** Cavitation erosion as the main cause of the flow leakage at the welding part: (a) cross-section of the leakage part [1]; Reproduced from [1], Korea Hydro & Nuclear Power: 2018. (b) schematic diagram for the cavitation erosion mechanism [1]; Reproduced from [1], Korea Hydro & Nuclear Power: 2018 and (c) flow leakage at the welding part [2]. Reproduced from [2], Korea Society for Fluid Machinery: 2019.

Cavitation may happen inside the orifice or the connecting pipe due to the flow acceleration occurring while passing through the orifice hole and the accompanying pressure drop, and as a result, performance degradation and structural damage of the orifice assemblies come about because of high-frequency vibration and material erosion. Cavitation

involves complex turbulent multiphase flows, so accurate simulation of these types of flows using available computational fluid dynamics (CFD) software remains a great challenge. In addition, it may be necessary for regulators to appropriately utilize the flow analysis results for the structural analysis in order to make reasonable regulatory decisions when reviewing licensing documents related to the structural integrity evaluation including cavitation effects.

Until recently, there have been very few experimental and numerical studies for the flow characteristics inside the multi-stage orifice. Wang et al. [3] experimentally investigated the inlet and outlet pressure drop characteristics for the multi-stage letdown orifice of the chemical and volume control system (CVCS) and designed the structure of the multi-stage orifice capable of providing a higher pressure drop without cavitation. The pressure drop could be improved by reducing the hole diameter of the orifice inlet or outlet, and the inlet pressure drop control method could produce a higher pressure drop compared to the outlet pressure drop control method. Bai et al. [4] numerically examined the effects of outlet pressure, the circular bead of the orifice inlet, and the change in the shape of the orifice outlet caused by the cavitation erosion on the cavitation characteristics inside the letdown orifice of the CVCS using ANSYS FLUENT. They found that when the inlet pressure was constant, cavitation did not occur in the letdown orifice unless the outlet pressure decreased to a specific value [4]. Once cavitation was formed in the letdown orifice, the degree of cavitation increased as the outlet pressure decreased [4]. The change in the shape of the orifice outlet caused by cavitation erosion significantly enhanced the degree of subsequent cavitation around the outlet of the letdown orifice [4]. Additionally, this effect was reinforced with the increase of shape change [4]. Niyogi et al. [5] confirmed using ANSYS FLUENT whether the performance of an eleven-stage orifice, designed to limit flow rate and prevent cavitation from occurring, was satisfactory. As a result of the simulation, the flow rate passing through the multi-stage orifice was limited to  $\pm 8\%$  of the nominal flow rate, and cavitation did not occur. However, even though the analysis model was three-dimensional geometry, two-dimensional axisymmetric flow analysis was performed, and three-dimensional flow analysis was limited to only three stages out of eleven stages. Araoye et al. [6] assessed the effect of the inlet velocity, orifice size, and spacing between orifices on the axial velocity and pressure distribution inside the two-stage orifice using ANSYS FLUENT. They found that the flow characteristics downstream of the two-stage orifice was qualitatively similar to that of a single-stage orifice in terms of the presence of recirculation and reattachment zone, and the shear layer region while some different flow structures, for examples a jet-type flow in the core region surrounded by donut-shaped vertical flow, were identified in the upstream of the second-stage orifice [6].

Insufficient understanding of the complex flow pattern (including cavitation) inside the multi-stage orifice, important to safe NPP operation, makes it difficult for the NPP operator or regulator to predict the pressure drop, cavitation, and erosion characteristics depending on either the operation condition or orifice geometry. To solve this difficulty, the main contents and scope of this study were composed as follows:

- To verify whether the numerical modeling available in ANSYS CFX R19.1 can predict reliably and accurately the complex flow inside the multi-stage orifice, the numerical analysis was performed on the six-stage orifice test facility, and the simulation results were compared with the measured data.
- To assess the adequacy of the changed operating flow rate proposed by a domestic NPP operator as the corrective measure about the flow leakage in the AFW pump recirculation line, the pattern of the cavitation flow in the eight-stage orifice and the connecting pipe depending on the magnitude of the operating flow rate was predicted by using ANSYS CFX R19.1.
- Using ANSYS Mechanical, the structural analysis was conducted for the eight-stage orifice and the connecting pipe under the same operating flow rate condition used for the flow analysis, and the structural integrity was evaluated for the allowable stress.

Additionally, modal analysis was performed to predict the possible occurrence of cavitation due to a pressure fluctuation.

- The geometric dimensions and arrangement of orifice hole position at the individual stage of the multi-stage orifice may have a significant influence on the characteristics of pressure drop and flow patterns (including cavitation). Therefore, these effects were examined by simulating an analysis model in which the hole diameter of the eighth stage orifice was changed under the design flow condition.

## 2. Validation of the Numerical Modeling

To validate whether the numerical modeling available in ANSYS CFX R19.1, predicts reliably and accurately the complex flow inside the multi-stage orifice, the numerical simulation was performed on the six-stage orifice and then the calculated pressure drop between inlet and outlet sections of the multi-stage orifice depending on the operating flow rate was compared with the measured data. For reference, the numerical modeling in this section was successfully validated for the single-stage orifice flowmeter [7].

### 2.1. Analysis Model

The analysis model in this section is based on a single-phase pressure drop test in a multi-stage letdown orifice pipe, performed by Wang et al. [3] of Shanghai University of Science and Technology. For reference, the multi-stage orifice installed in the NPP is generally operated at high pressure and the local flow velocity passing through the orifice hole may exceed 100 m/s. Therefore, it is difficult to find detailed experimental data to validate the simulation results for multiphase flow including cavitation. Figure 3 shows the schematic diagram of the multi-stage orifice used as the test apparatus. The corresponding multi-stage orifice consisted of six stages and the total length was 700 mm (For reference, the total length of the present analysis model was extended to 990 mm to guarantee no reverse flow at the outlet boundary). The length ( $L_s$ ) between the five orifice disks (or plates) located on the upstream side was equal to 101.6 mm respectively. The sixth stage orifice disk had a hole in the pipe centerline and was connected to the remaining upstream five orifice stages by two flanges. In addition, the sixth stage orifice disk can be easily replaced by a disk having a different orifice hole diameter [3]. Particularly, the orifice holes from the second to the fifth stage were alternately and eccentrically arranged in the opposite direction from the pipe centerline.

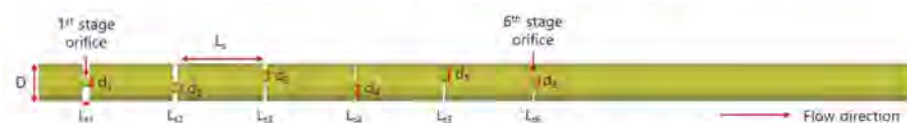


Figure 3. Schematic diagram of the six-stage orifice.

The main geometrical dimensions of the multi-stage orifice were summarized in Table 1. Here,  $L_t$  is the thickness of the orifice disk, and  $\beta$  is the ratio of the orifice hole diameter ( $d$ ) to the inner diameter of the connecting pipe ( $D$ ). The diameter ratio increased from the first to fifth stage orifice, while the sixth stage orifice showed a smaller magnitude than the fourth stage orifice.

Table 1. The geometrical information for six-stage orifice [3].

Stage No.	$L_t$ (mm)	$d$ (mm)	$D$ (mm)	$\beta = d/D$
1	9.0	10.31	42.82	0.241
2	6.0	12.14		0.284
3	4.0	14.27		0.333
4	3.0	16.69		0.390
5	3.0	19.30		0.451
6	3.0	15.00		0.350

The flow rate was supplied using a ten-stage centrifugal pump with a rated flow rate of 5.0 m<sup>3</sup>/h and maximum discharge pressure of 1.9 MPa [3]. The test flow rate was adjusted using a butterfly valve installed downstream of the connecting pipe [3]. The pressure drop between the orifice inlet and outlet was calculated using the measured data obtained through a series of repeated tests [3]. Water at 54.4 °C was used as the working fluid.

## 2.2. Numerical Modeling

In this study, the turbulent flow inside the six-stage orifice was calculated under steady, single-phase, and incompressible flow conditions using ANSYS CFX R19.1. The spatial discretization error may be caused by the accuracy order of the difference scheme and grid spacing. For either flow that is not parallel to the grid line or complex flows, it is recommended not to use the discretization scheme with the first-order accuracy [8]. Therefore, in the present study, the convective terms of the momentum and turbulence transport equations were calculated by applying the high-resolution scheme equivalent to the second-order accuracy. For reference, in the high-resolution scheme, the values of the blend factor are determined using the local solution for the entire computational domain. For flow regions where the gradient of the variable is small, the blend factor has a value close to 1 and as a result, this scheme has the second-order accuracy. In the case of flow regions where the gradient of the variable changes rapidly, the blend factor has a value close to 0 and consequently this scheme has the first-order accuracy to prevent distortion of the simulation result and maintain robustness. When the root mean square residual of the individual equations was 10<sup>-5</sup> or less and the change of the main variables was very small, the calculation was judged to be converged.

In CFD simulations, the types of errors can be divided into numerical errors and model errors. The turbulence model is one of the main causes of model error. In general, the flow patterns are quite complex in the issues related to IST, but no turbulence model can accurately simulate them throughout the whole computational domain. In this study, the turbulent flow inside the multi-stage orifice was calculated applying the standard k-ε model widely used in the industry among the turbulence models based on the Reynolds-averaged Navier–Stokes (RANS) equation available in ANSYS CFX R19.1. Differential transport equations for the turbulence kinetic energy (*k*) and turbulence dissipation rate (*ε*) are as follows:

$$\frac{\partial(\rho k)}{\partial t} + \frac{\partial}{\partial x_i}(\rho k U_i) = \frac{\partial}{\partial x_j} \left[ \left( \mu + \frac{\mu_t}{\sigma_k} \right) \frac{\partial k}{\partial x_j} \right] + P_k - \rho \epsilon \quad (1)$$

$$\frac{\partial(\rho \epsilon)}{\partial t} + \frac{\partial}{\partial x_i}(\rho \epsilon U_i) = \frac{\partial}{\partial x_j} \left[ \left( \mu + \frac{\mu_t}{\sigma_\epsilon} \right) \frac{\partial \epsilon}{\partial x_j} \right] + \frac{\epsilon}{k} (C_{\epsilon 1} P_k - C_{\epsilon 2} \rho \epsilon) \quad (2)$$

$$\mu_t = \rho C_\mu \frac{k^2}{\epsilon} \quad (3)$$

where *U<sub>i</sub>* is the mean velocity components, *ρ* is the fluid density, *μ* is the molecular (or dynamic) viscosity, *C<sub>μ</sub>* = 0.09, *C<sub>ε1</sub>* = 1.44, *C<sub>ε2</sub>* = 1.92, *σ<sub>k</sub>* = 1.0, and *σ<sub>ε</sub>* = 1.3 are turbulence constants and *μ<sub>t</sub>* is the turbulent (or eddy) viscosity. *P<sub>k</sub>* is the production of turbulence kinetic energy due to the mean velocity gradient. The standard k-ε model is numerically stable and has a well-established flow regime with good predictive performance, so it has been adopted by most general-purpose CFD software and used as a representative turbulence model in the related industries. However, this model may have limitations in accurately predicting boundary layer separation, flow accompanying rapid changes in the average strain rate, rotational flow, and flow over the curved surfaces [9].

As shown in Figure 4, the computational grid in the form of an unstructured hexahedron was generated using the ICEM-CFD, grid generation software, for the same sized computational domain as the test facility. The total number of computational nodes used in



the calculation was about  $7.58 \times 10^6$ . For reference, detailed information on the grid system used in the calculation was summarized in Table 2. The full geometry of the six-stage orifice was considered in case the flow could not maintain the symmetrical pattern when passing through the orifice hole. Additionally, in order to properly predict the complex turbulent flow inside the orifice, a dense grid distribution was applied near the wall and the orifice hole.

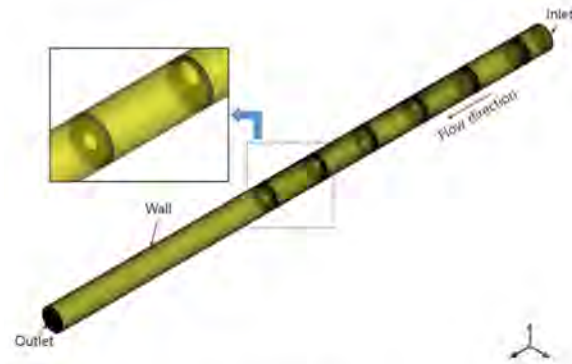


Figure 4. Grid system for six-stage orifice.

Table 2. Grid information for six-stage orifice.

Items	Values	Items	Values
Total number of nodes	$7.58 \times 10^6$	Max. face angle	135.0°
Total number of elements	$7.48 \times 10^6$	Max. edge length ratio	771.7
Min. face angle	45.0°	Max. element volume ratio	18.8

As the inlet boundary condition, the velocity profile for the fully developed flow obtained through the separate flow analysis applying the corresponding flow conditions for the orifice-free pipe with the same pipe diameter and turbulence intensity of 5% were applied. Average static pressure was used as the outlet condition. The walls were assumed to be smooth with zero surface roughness and a no-slip condition was applied there. A scalable wall function was applied to calculate the flow near the wall. This wall function can solve one of the main problems of the standard wall function in that it can be applied to any dense grid without resulting in the erroneous modeling of the laminar and buffer regions of the boundary layer.

### 2.3. Validation Results

Figure 5a shows the pressure sampling points at seven locations of the multi-stage orifice.  $P_0$  and  $P_6$  represent pressure sampling points located at the inlet and outlet of the multi-stage orifice, respectively, and their positions were approximately 30 mm away from the adjacent orifice disk. The remaining five pressure sampling points,  $P_1$  to  $P_5$ , were located downstream from the adjoining orifice disk by a distance of  $3d_1 \sim 3d_5$ , respectively. Figure 5b shows the result of comparing the calculated pressure drop ( $\Delta p = P_0 - P_6$ ) between the inlet and outlet sections of the multi-stage orifice with the measured data depending on the inlet flow rate. As the inlet flow rate increased, the magnitude of the pressure drop also increased, and the predicted static pressure drop in the range of the inlet flow rate  $5.24 \sim 6.21 \text{ m}^3/\text{h}$  was consistent within a maximum deviation of 5% compared to the measurement results. However, the gradient between the measured inlet flow rate and pressure drop decreased as the flow rate became smaller, while the predicted result maintained an almost constant gradient. In this regard, it was confirmed that the Reynolds number based on both pipe diameter and the mean inlet velocity at an inlet flow rate of  $5.24 \text{ m}^3/\text{h}$  was  $8.68 \times 10^4$  (Reynolds number for the other inlet flow rates can be found

in Table 3), which corresponded to a completely turbulent flow, but the reason for the decrease in the gradient between the measured inlet flow rate and pressure drop could not be found.

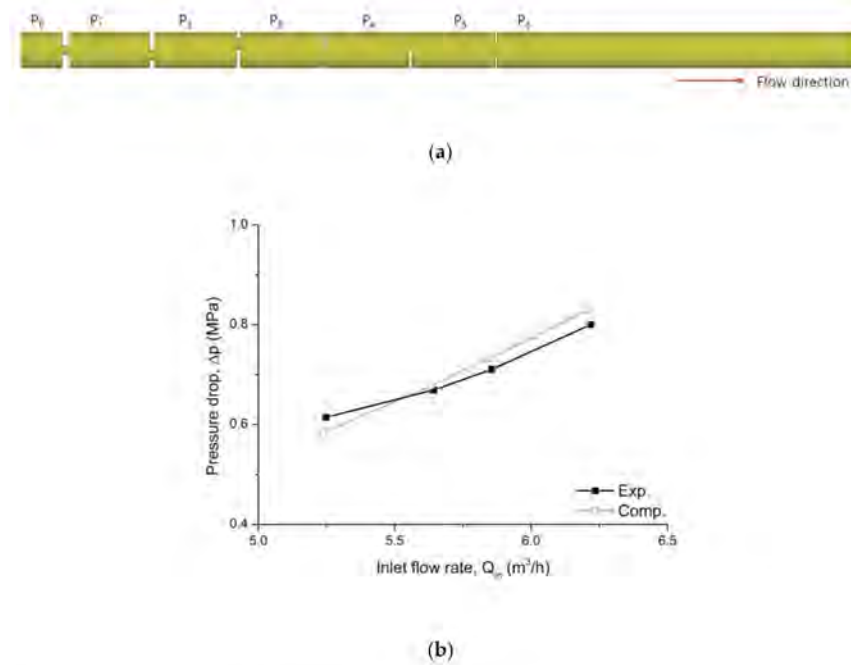


**Figure 5.** Comparison of measured and predicted static pressure drop versus inlet flow rate: (a) pressure sampling points and (b) static pressure drop versus inlet flow rate.

**Table 3.** Pressure drop between each orifice stage.

Flowrate (m <sup>3</sup> /h)	Reynolds Number	P <sub>0</sub> –P <sub>1</sub> (MPa)	P <sub>1</sub> –P <sub>2</sub> (MPa)	P <sub>2</sub> –P <sub>3</sub> (MPa)	P <sub>3</sub> –P <sub>4</sub> (MPa)	P <sub>4</sub> –P <sub>5</sub> (MPa)	P <sub>5</sub> –P <sub>6</sub> (MPa)
5.24	$8.68 \times 10^4$	0.25	0.11	0.08	0.046	0.027	0.067
5.64	$9.32 \times 10^4$	0.29	0.13	0.09	0.055	0.031	0.08
5.85	$9.67 \times 10^4$	0.31	0.14	0.1	0.06	0.034	0.086
6.02	$9.96 \times 10^4$	0.33	0.15	0.11	0.062	0.035	0.09
6.21	$1.03 \times 10^5$	0.35	0.16	0.12	0.065	0.038	0.096

On the other hand, as shown in Table 3, the smaller the orifice hole diameter, the higher the flow velocity, so the magnitude of the pressure drop at the individual orifice stage was correspondingly in the order of 1st > 2nd > 3rd > 6th > 4th > 5th stage orifice.

Besides the validation for the calculation results, the distribution of the predicted flow velocity and streamline inside the multi-stage orifice can be found in the author's research report [10].

### 3. Effect of the Operating Flow Rate

As previously shown in Figures 1 and 2, flow leakage due to cavitation erosion happened at the socket welding part downstream of the multi-stage orifice installed in the AFW pump recirculation line. As the corrective measure, the domestic NPP operator changed the operating flow rate to prevent the occurrence of cavitation flow. To assess the appropriateness of this corrective action, the audit calculation from the regulatory perspective was conducted by using ANSYS CFX R19.1, and simulation results were explained in this section.

### 3.1. Analysis Model

The analysis model is a multi-stage orifice installed in the recirculation line of the AFW pump to limit the flow rate at the high discharge pressure of the AFW pump and to decompress the corresponding system. Figure 6 shows the schematic diagram of the multi-stage orifice and the connecting pipe. The multi-stage orifice consisted of eight stages. The first and eighth stage orifice had holes in the center of the pipe, while the second to seventh stage orifice were alternately and eccentrically arranged in the opposite direction from the pipe centerline. Hole diameter ( $d$ ), the spacing between the orifice disks ( $L_s$ ), and thickness of orifice disk ( $L_t$ ) for each orifice stage were the same. Since the quantitative dimensions of the multi-stage orifice were related to the intellectual property rights of the manufacturer, specific information could not be provided. Water at 40 °C was used as the working fluid.



Figure 6. Schematic diagram of the eight-stage orifice and the connecting pipe.

As previously shown in Figure 1, the recirculation line is opened when the NPP is in the mode of start/stop transient or the AFW pump is operated while the AFW pump outlet valve in the MFW line is closed. As the pressure in the steam generator side decreases, the recirculation flow rate is determined by the system resistance–pump performance matching characteristics. The minimum (or design) flow rate for the safe operation of the AFW in the recirculation line is about 19.3 m<sup>3</sup>/h, and a maximum operation time of a quarter-hour is allowed [11]. On the other hand, the minimum flow rate for continuous safe operation without stopping the AFW pump was about 34.1 m<sup>3</sup>/h.

### 3.2. Numerical Modeling

#### 3.2.1. Flow Analysis

In this study, the turbulent flow inside an eight-stage orifice was calculated using ANSYS CFX R19.1 under steady, multiphase, and incompressible flow conditions. The discretization accuracy for the convective terms of the momentum equation and turbulence transport equation, turbulence model, grid type, and so on were the same as those described in Section 2.2. The mixture model was used to consider an interphase transfer. This model solves the continuity, momentum, energy equation for the mixture, and the volume fraction equation for the secondary phase (vapor). For the cavitation flow simulation, liquid–vapor mass transfer is governed by the following the vapor volume fraction equation:

$$\frac{\partial(\rho_v \alpha_v)}{\partial t} + \frac{\partial}{\partial x_i}(\rho_v \alpha_v v_i) = R_{vap} - R_{cond} \quad (4)$$

where  $\rho_v$  is the vapor density,  $\alpha_v$  is the vapor volume fraction, and  $v_i$  is the directional velocity component,  $R_{vap}$  and  $R_{cond}$  are the mass transfer rates correspond to the vaporization and condensation during the cavitation process respectively. The Rayleigh–Plesset equation describing the bubble growth in the liquid is given by:

$$R_{vap} = F_{vap} \frac{3\alpha_n(1 - \alpha_v)\rho_v}{R_B} \sqrt{\frac{2}{3} \frac{(p_v - p)}{\rho_l}}, p < p_v \quad (5)$$

$$R_{cond} = F_{cond} \frac{3\alpha_v\rho_v}{R_B} \sqrt{\frac{2}{3} \frac{(p - p_v)}{\rho_l}}, p > p_v \quad (6)$$

where  $R_{nuc} = 10^{-6}$  m is the nucleation site radius,  $p_v$  is the vapor pressure at the liquid temperature,  $p$  is the liquid pressure,  $\rho_l$  is the liquid density,  $\alpha_n = 5 \times 10^{-4}$  is the volume



fraction of the nucleation sites, and  $F_{vap} = 50$  and  $F_{cond} = 0.01$  are an empirical factor depend on vaporization and condensation designed for the different rates (vaporization is generally much faster than condensation). Saturation pressure set to about 7.36 kPa. For reference, the numerical method used in this study was summarized in Table 4. According to the author's previous study [12,13], the numerical modeling explained in this section reliably predicted the cavitation flow occurring inside the IST-related components (e.g., cavitating Venturi and sharp-edged orifice).

**Table 4.** Numerical method.

Items	Contents
Discretization accuracy for the convective terms	High resolution
Momentum eqn.	High resolution
Turbulence transport eqn.	Mixture
Interphase transfer model	Rayleigh–Plesset
Cavitation model	Standard k- $\epsilon$
Turbulence model	Scalable wall function
Near-wall treatment method	$<10^{-5}$
Convergence criterion	

On the other hand, to obtain accurate simulation results when calculating cavitation flow using CFD software, it is essential to consider an appropriate grid type, especially at the location where cavitation may occur. In this regard, the authors confirmed through a previous study [14] that the grid shape had a significant effect on the cavitation analysis results (cavitation inception condition, discharge coefficient magnitude, etc.) inside a sharp-edged orifice. Based on the results of the previous study, to properly predict the cavitation flow inside the multi-stage orifice, a dense grid distribution was applied near the wall and the orifice hole as shown in Figure 7.

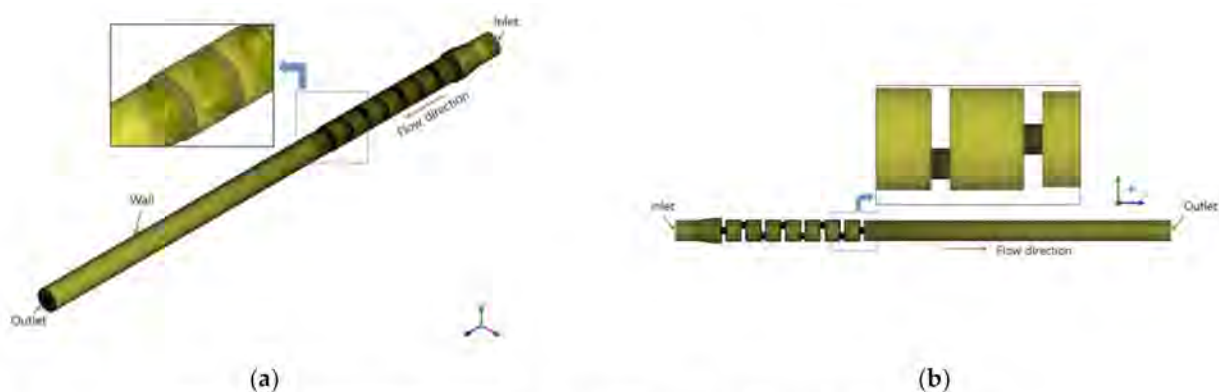


**Figure 7.** Grid system for eight-stage orifice: (a) isometric-view and (b) x-axis view.

In addition, as shown in Table 5, a grid sensitivity study was performed for three types of grid systems. Type1 was the coarsest grid, and Type2 and 3 had dense grids near walls and orifice holes. Overall, the difference in the analysis results depending on the grid size was not large, and to understand in more detail the complex flow field (including cavitation flow) inside the multi-stage orifice with the reasonable computation cost, the prediction results for an intermediate grid (Type2, total number of nodes:  $5.02 \times 10^6$ ) were explained in this paper.

Operating flow rate ( $Q_{in} = 34.1, 37.0, 39.0,$  and  $41.5 \text{ m}^3/\text{h}$ ), turbulence intensity of 5%, and eddy viscosity ratio of 10 were applied as inlet conditions. The volume fraction of the liquid phase (water) at the inlet was assumed to be 1. As an outlet condition, the measured gauge pressure of about 310 kPa was used. The walls were assumed to be smooth and no-slip condition was applied there. A scalable wall function was applied to calculate the flow near the wall.

**Table 5.** Grid information.

Items	Type1	Type2	Type3
Total number of nodes	$3.21 \times 10^6$	$5.02 \times 10^6$	$7.04 \times 10^6$
Total number of elements	$3.15 \times 10^6$	$4.94 \times 10^6$	$6.94 \times 10^6$
Min. face angle	45.3°	45.2°	45.2°
Max. face angle	134.9°	135.0°	135.0°
Max. edge length ratio	611.6	61.3	61.3
Max. element volume ratio	9	9	9

### 3.2.2. Structural Analysis

Figure 8 shows the geometry modeling for the structural analysis of an eight-stage orifice made by ANSYS SpaceClaim. In addition to the geometry modeling for flow analysis shown in Figure 6, the actual thickness and the welding parts between the multi-stage orifice and the connecting pipes were considered. However, the thinning of the welding part due to cavitation erosion was not considered in this study.

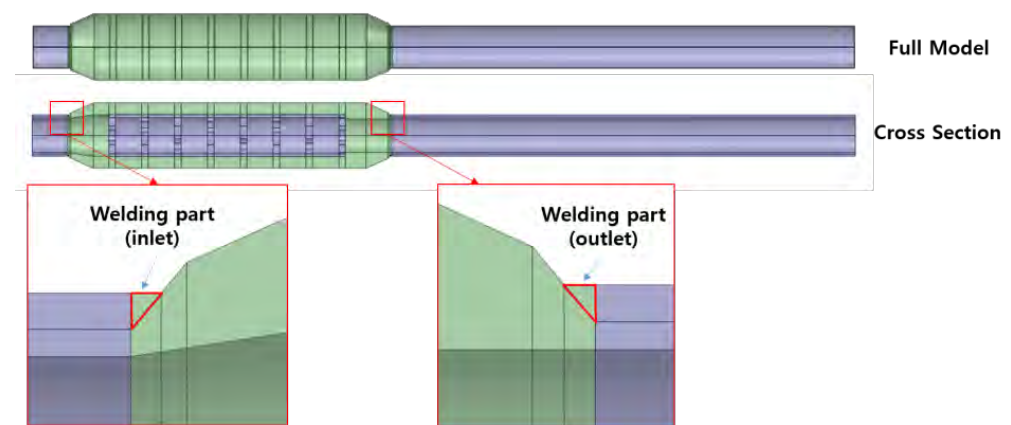
**Figure 8.** Geometry modeling for the structural analysis of the eight-stage orifice.

Figure 9 shows the grid shape for the structural analysis of an eight-stage orifice generated using ANSYS Meshing. To improve the accuracy of the analysis model, a 3D SOLID element representing quadratic displacement behavior was applied. The element has three degrees of freedom per node and provides plasticity, hyperelasticity, creep, stress stiffening, large deflection, and strain [15]. To assess the sensitivity depending on the element size, the structural analysis was performed by changing the default element size to 1.5, 2.5, and 3.0 mm.

As shown in Figure 10, the predicted stress intensity at the same location was compared. As the total number of nodes increased, the rate of change in the magnitude of stress intensity was reduced, and the tendency to converge to a constant value was shown. Based on the results of the grid sensitivity study as described above, the default element size for the structural analysis of an eight-stage orifice was determined to be 1.5 mm.

As shown in Figure 11, the material property values were applied by referring to ASME Code Section-II, Part-D. In the case of the welding part, stainless steel property was used.

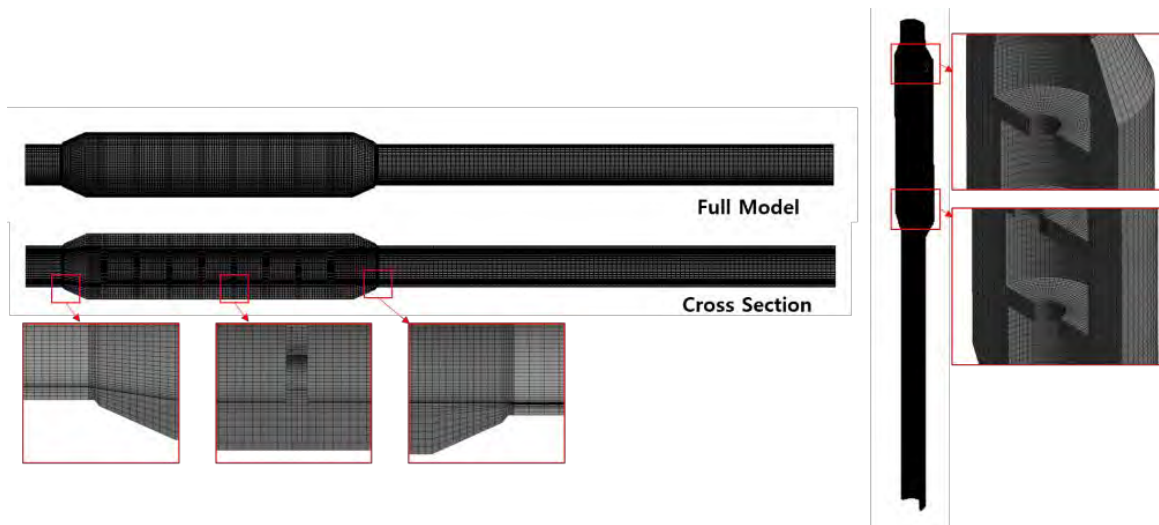


Figure 9. Grid system for the structural analysis of the eight-stage orifice.

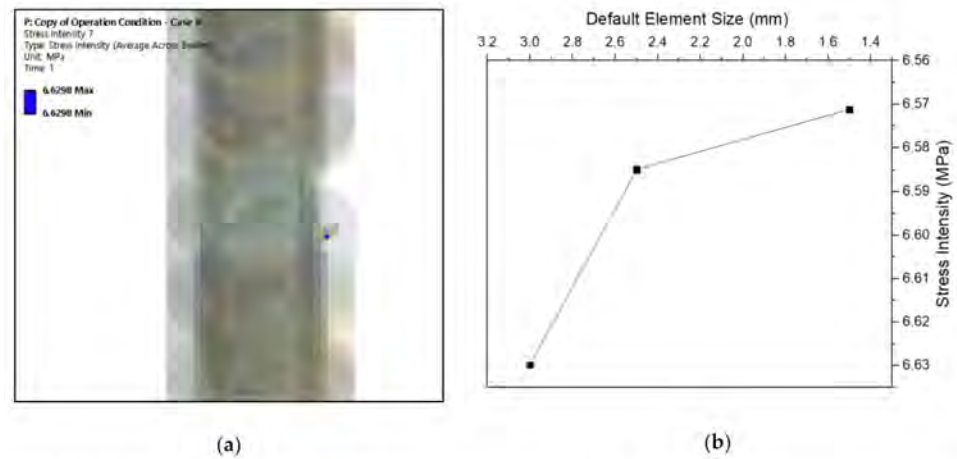


Figure 10. Results of the grid sensitivity study for the structural analysis: (a) location for the assessment of stress intensity and (b) default element size versus stress intensity.

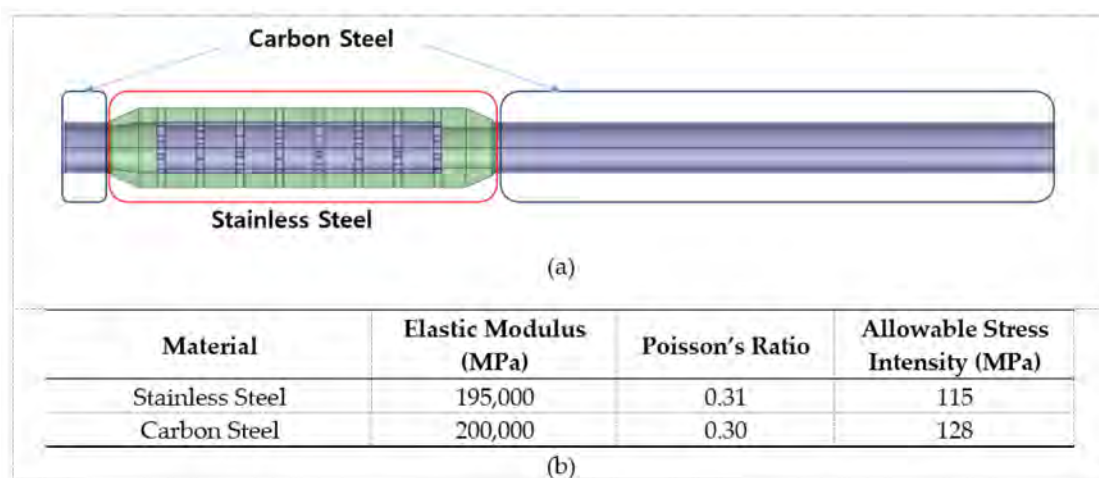


Figure 11. Material properties values per zone: (a) type of material properties applied per zone and (b) material properties values.

As shown in Figure 12, constraints were applied to the cross-sections of the upstream and downstream connecting pipes of the multi-stage orifice. Specifically, in the upstream pipe, the degrees of freedom in the hoop and axial directions were fixed, but the degree of freedom in the radial direction was free. On the other hand, in the downstream pipe, the degree of freedom in the hoop direction was fixed, but the degrees of freedom in the radial and axial directions were free. The flow analysis results obtained using ANSYS CFX R19.1 were applied as the pressure boundary condition at the inner wall of the multi-stage orifice and the connecting pipe. To be more specific, the Program Controlled Mapping option was selected to transfer the wall pressure data across a dissimilar mesh interface, that is, from ANSYS CFX to ANSYS Mechanical. This option can determine the appropriate settings based on the source and target mesh, and the data transfer type.



Figure 12. Constraint conditions.

### 3.3. The Computational Results

#### 3.3.1. Flow Analysis

Figure 13a shows the distribution of the vapor volume fraction in the second half of the multi-stage orifice depending on the operating flow rate.

As the operating flow rate increased, the region with a vapor volume fraction of 0.9 or more expanded to the downstream of the eighth stage orifice. In fact, at  $41.5 \text{ m}^3/\text{h}$ , a flow rate condition in which leakage in the welding part due to cavitation erosion really occurred, a cavitation flow region was widely formed downstream of the eighth stage orifice. Besides, cavitation flow still appeared around the hole of the eighth stage orifice even at  $34.1 \text{ m}^3/\text{h}$ , corresponded to not only the operating flow rate that the NPP operator suggested as the corrective measure but also the minimum flow rate required for continuous safe operation without stopping the AFW pump.

Figure 14 shows the distribution of flow velocity and streamlines inside the eight-stage orifice and the connecting pipe (for the symmetric  $y$ - $z$  plane) depending on the operating flow rate. The flow patterns between the sixth to seventh and seventh to eighth stage orifices were similar regardless of the magnitude of the operating flow rate. However, as the operating flow rate increased, the peak value of flow velocity also increased, and the high-speed jet flow region passing through the hole of the eighth stage orifice tended to expand. In addition, since the flow passing through the hole of the eighth stage orifice was directed to the upper part of the connecting pipe, the primary recirculation flow was formed at the lower part of the jet flow.

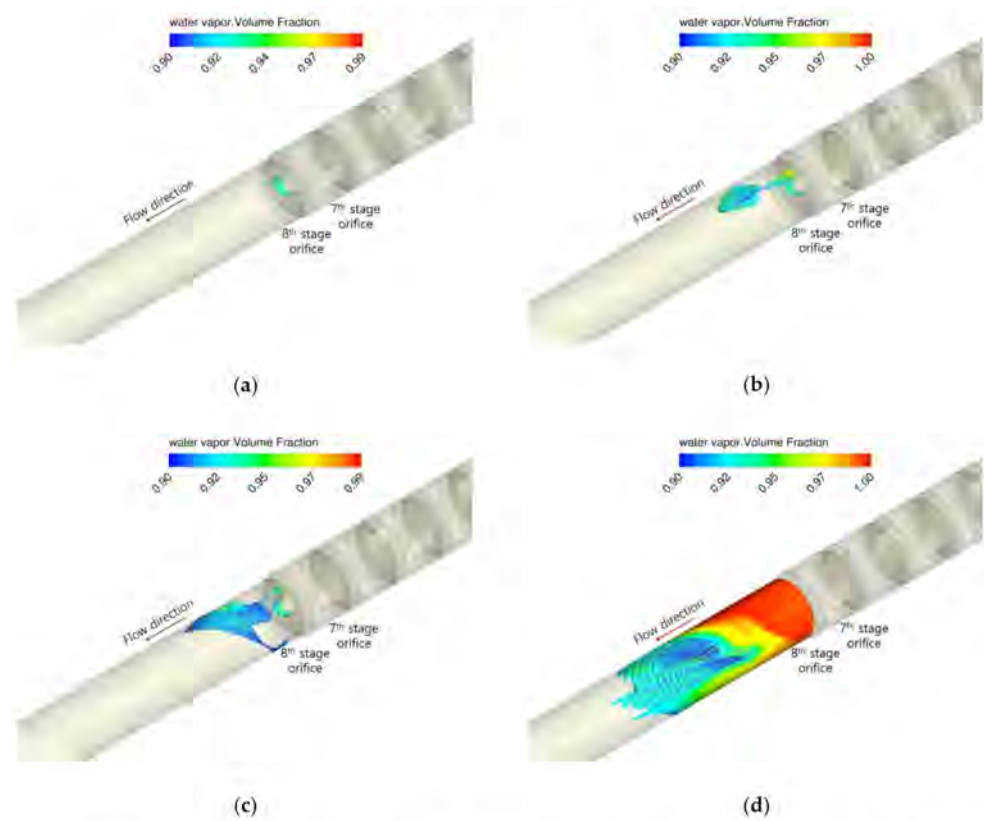


**Figure 13.** Iso-volume of vapor volume fraction: (a)  $Q_{in} = 34.1 \text{ m}^3/\text{h}$  ( $Re = 2.74 \times 10^5$ ); (b)  $Q_{in} = 37.0 \text{ m}^3/\text{h}$  ( $Re = 2.97 \times 10^5$ ); (c)  $Q_{in} = 39.0 \text{ m}^3/\text{h}$  ( $Re = 3.13 \times 10^5$ ); and (d)  $Q_{in} = 41.5 \text{ m}^3/\text{h}$  ( $Re = 3.33 \times 10^5$ ).

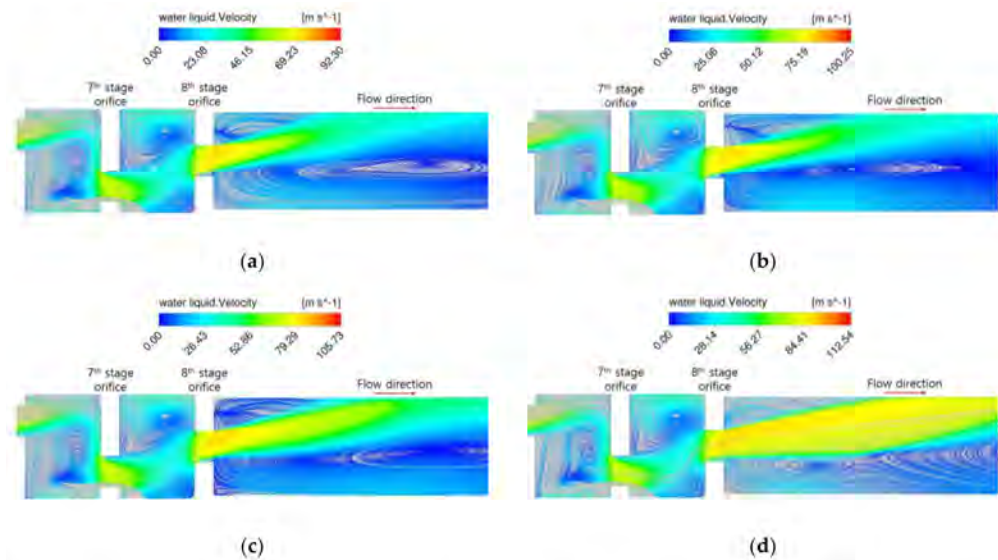


**Figure 14.** Distribution of flow velocity and streamlines inside the eight-stage orifice and the connecting pipe (for the symmetric y-z plane) depending on the operating flow rate: (a)  $Q_{in} = 34.1 \text{ m}^3/\text{h}$  ( $Re = 2.74 \times 10^5$ ); (b)  $Q_{in} = 37.0 \text{ m}^3/\text{h}$  ( $Re = 2.97 \times 10^5$ ); (c)  $Q_{in} = 39.0 \text{ m}^3/\text{h}$  ( $Re = 3.13 \times 10^5$ ); and (d)  $Q_{in} = 41.5 \text{ m}^3/\text{h}$  ( $Re = 3.33 \times 10^5$ ).

Figure 15 shows the mass-averaged vapor volume fraction in the seventeen axial cross-sections (6.35 mm spacing between cross-sections) downstream of the eighth stage orifice depending on the operating flow rate. The mass-averaged vapor volume fraction of



the corresponding cross-sections also increased as the operating flow rate increased except for the cross-section number from 1 to 4 in the case of the operating flow rate of 37.0 m<sup>3</sup>/h condition. On the other hand, at 41.5 m<sup>3</sup>/h, which is a flow condition in which leakage occurred at the welding part of the multi-stage orifice and the connecting pipe due to cavitation erosion, the mass-averaged vapor volume fraction from cross-section number 13 to 14 showed the maximum value. These cross-sections corresponded to the location where flow leakage appeared. Therefore, it may be judged that the simulation results obtained by applying the numerical modeling described in Section 3.2.1 can properly reflect the actual situation where the leakage occurred.

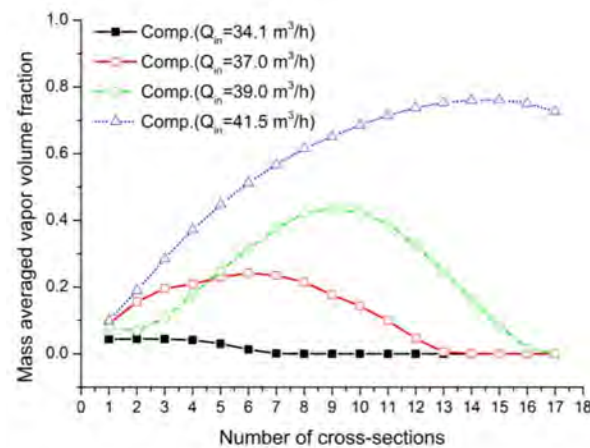


**Figure 15.** The mass-averaged vapor volume fraction in the axial cross-sections downstream of the eighth stage orifice depending on the operating flow rate.

Based on the above-mentioned flow analysis results, it was confirmed that the operating flow rate was the main factor to influence the cavitation behavior inside the multi-stage orifice. Therefore, the reduction in the operating flow rate suggested by the NPP operator is judged to be an appropriate corrective action. However, it was found that cavitation still happened in the vicinity of the changed operating flow rate of 34.1 m<sup>3</sup>/h, i.e., minimum flow rate required for the continuous safe operation of the AFW pump. Therefore, as an additional measure, it is necessary to shorten the operating time of the AFW pump and reinforce periodic monitoring (vibration measurement during the AFW pump operation) [1]. Separately, it is required to review the design appropriateness of the multi-stage orifice as a fundamental solution to prevent flow leakage from the welding part between the multi-stage orifice and the connecting pipe caused by cavitation erosion.

### 3.3.2. Structural Analysis

Table 6 and Figure 16 show the predicted results of the stress intensity distribution in the multi-stage orifice and the connecting pipes depending on the operating flow rate by applying the numerical modeling for the structural analysis, described in Section 3.2.2, to ANSYS Mechanical. As the operating flow rate increased, the maximum value of the stress intensity also increased. The maximum value of the stress intensity occurred in the upstream connecting pipe of the multi-stage orifice, which is believed to be due to the depressurization occurring as the flow entered into the multi-stage orifice passed through the orifice hole. On the other hand, it was not evident whether the high-stress intensity caused by cavitation flow occurred in the welding part between the multi-stage orifice and the connecting pipe.

**Table 6.** The predicted results of stress components depending on the operating flow rate.

Case	Flowrate (m <sup>3</sup> /h)	Diameter Ratio (d <sub>g</sub> /d)	Stress Intensity (MPa)	Membrane Stress (MPa)	Membrane + Bending Stress (MPa)	Allowable Stress (MPa)	Location of Maximum Stress
OP1	34.1	1	123.6	105.9	121.8	207	Upstream connecting pipe
OP2	37		145.8	125	143.7		
OP3	39		162	138.8	159.7		
OP4	41.5		183.8	157.5	181.2		

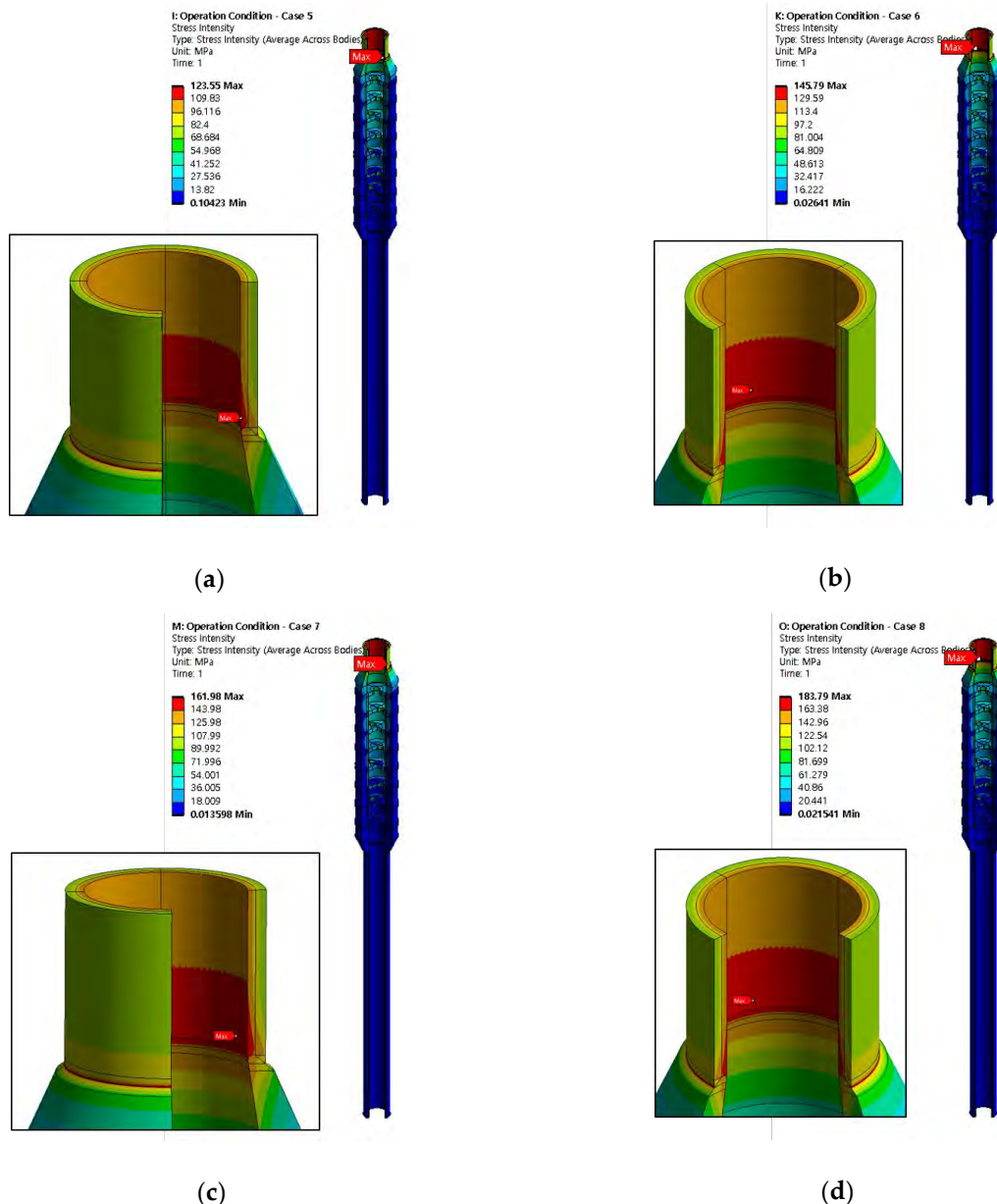


**Figure 16.** Distribution of the predicted stress intensity depending on the operating flow rate: (a)  $Q_{in} = 34.1 \text{ m}^3/\text{h}$  ( $Re = 2.74 \times 10^5$ ); (b)  $Q_{in} = 37.0 \text{ m}^3/\text{h}$  ( $Re = 2.97 \times 10^5$ ); (c)  $Q_{in} = 39.0 \text{ m}^3/\text{h}$  ( $Re = 3.13 \times 10^5$ ); and (d)  $Q_{in} = 41.5 \text{ m}^3/\text{h}$  ( $Re = 3.33 \times 10^5$ ).

In summary, the analysis result of the stress intensity distribution in the multi-stage orifice and the connecting pipe depending on the operating flow rate showed a value less than the allowable stress of 207 MPa. Therefore, the decrease in the operating flow rate suggested by the NPP operator is considered to be reasonable in that it can secure more

margins for the structural integrity of the corresponding facility, including the welding part between the multi-stage orifice and the connecting pipe. As described above, since the maximum value of the stress intensity occurred in the connecting pipe upstream of the multi-stage orifice, it will be expected that the above-mentioned analysis result will not change significantly even if the additional structural analysis is performed by considering the thinning of the welding part between the multi-stage orifice and the connecting pipe due to cavitation erosion.

Table 7 shows the predicted deformation results for each direction in the multi-stage orifice and the connecting pipe depending on the operating flow rate. The deformation size in each direction also increased as the operating flow rate increased, except for the deformation in the hoop direction at  $Q_{in} = 37.0 \text{ m}^3/\text{h}$ . At the same operating flow rate, the amount of deformation for each direction was in the order of axial > radial > hoop. In the case of radial deformation, the maximum deformation value was shown in the upstream connecting pipe of the multi-stage orifice where high stress acted. For axial deformation, the maximum deformation value was shown at the seventh stage orifice. In the case of the deformation in the hoop direction, the maximum deformation value was shown either at the third stage orifice or in the downstream connecting pipe of the multi-stage orifice depending on the operating flow rate.

**Table 7.** The predicted results of deformation components depending on the operating flow rate.

Case	Flowrate (m <sup>3</sup> /h)	Diameter Ratio (d <sub>s</sub> /d)	Max. Radial Deformation (mm)	Location of Max. Deformation	Max. Hoop Deformation (mm)	Location of Max. Deformation	Max. Axial Deformation (mm)	Location of Max. Deformation
OP1	34.1	1	0.013	Upstream connecting pipe	0.0017	3rd stage orifice	0.0154	7th stage orifice
OP2	37		0.0155		0.0044	Downstream connecting pipe	0.0183	
OP3	39		0.0171	0.0023	3rd stage orifice	0.0203		
OP4	41.5		0.0194	0.0037	Downstream connecting pipe	0.0231		

Additionally, a modal analysis was performed to generate frequencies for the finite element model and the boundary conditions applied to the connecting pipe inlet and outlet ends. The first 20 modes were summarized in Figure 17, and some of the corresponding mode shapes were shown in Figure 18. From the mode shapes, it was found that the first seven beam modes ranged from 137 to 4321 Hz. Specifically, corresponding values of 1061 Hz and 1612 Hz were found for the third and fourth beam modes, between 1000 and 2000 Hz, which showed several peak values in the frequency domain resulting from cavitation at the specific flow rate [2]. This may be one of the reasons for a possible resonance effect between the structural frequency and the forcing frequency. Four radial modes were shown at 863 Hz, 2286 Hz, 3754 Hz, and 4661 Hz. Moreover, two axial modes were found at 1252 Hz and 2227 Hz for orifice modes with forward and backward motions of the flow direction, respectively. The modal characteristics obtained by the modal analysis give the possible solution to escape the peak values of pressure fluctuation between 1000 and 2000 Hz. Decreasing flow rate may be one of the options to eliminate resonance between the structural frequency and the cavitation frequency.

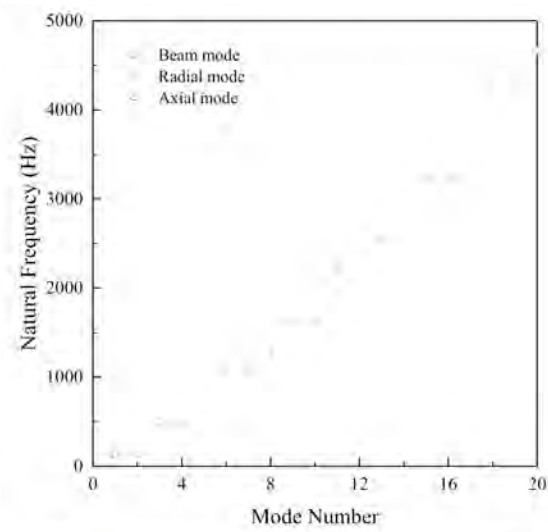


Figure 17. Natural frequencies of the multi-stage orifice and the connecting pipe.

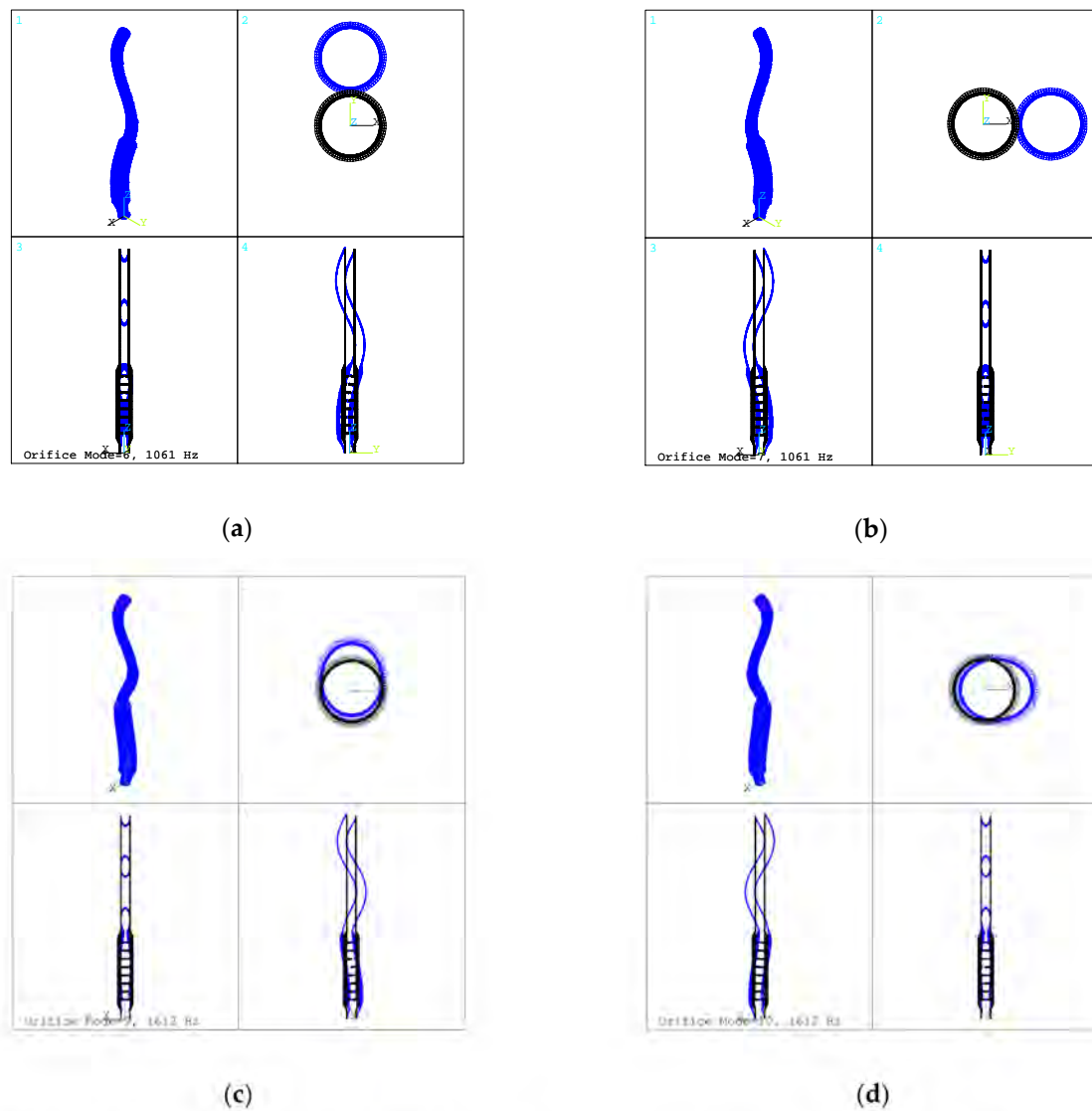


Figure 18. Mode shapes of the multi-stage orifice and the connecting pipe: (a)  $d_8/d = 0.84$ ; (b)  $d_8/d = 1.0$  (original case); (c)  $d_8/d = 1.24$ ; and (d)  $d_8/d = 1.49$ .

#### 4. Effect of the Orifice Hole Diameter Size

Apart from the variables related to the performance of the multi-stage orifice, an important design consideration is to ensure that cavitation does not occur inside the multi-stage orifice [5]. In this regard, the dimensions and arrangement positions of the orifice holes in individual stages of the multi-stage orifice can have a significant influence on the pressure drop characteristics and flow patterns (including cavitation). Therefore, in this section, the effect of the change in the hole diameter ( $d_8$ ) of the eighth stage orifice (shown in Figure 6) on the pressure drop characteristics and flow patterns was investigated.

##### 4.1. Analysis Model

The analysis model in this section additionally considered the cases that the ratio ( $d_8/d$ ) of the changed hole diameter ( $d_8$ ) to the existing hole diameter ( $d$ ) of the eighth stage orifice was 0.84, 1.24, and 1.49, respectively. In this case, the ratio ( $d_8/D$ ) of the hole diameter ( $d_8$ ) of the eighth stage orifice to the inner diameter ( $D$ ) of the upstream connecting pipe was 0.22, 0.32, and 0.38, respectively. Except for the hole diameter of the eighth stage orifice, the remaining geometric specifications were maintained. On the other hand, the simulation was performed on the design flow rate of about  $19.3 \text{ m}^3/\text{h}$  ( $Re = 1.53 \times 10^5$ ), which allows the safe operation of the AFW pump for a maximum of 15 min. The corresponding flow rate was the reduced amount up to 54% compared to the operating flow rate ( $Q_{in} = 34.1, 37.0, 39.0, \text{ and } 41.5 \text{ m}^3/\text{h}$ ) described in Section 3.2.1.

##### 4.2. Numerical Modeling

###### 4.2.1. Flow Analysis

Except for applying the design flow rate ( $Q_{in} = 19.3 \text{ m}^3/\text{h}$ ) as the inlet condition, the discretization scheme for the convective terms of the momentum and turbulence transport equation, turbulence model, multiphase flow model, grid shape, and boundary conditions were the same as those described in Section 3.2.1.

###### 4.2.2. Structural Analysis

Except that additional flow analysis result obtained using ANSYS CFX R19.1 for the change of both the hole diameter of the eighth stage orifice and the flow rate was applied as the pressure boundary condition on the inner wall of the multi-stage orifice and the connecting pipes, the grid shape, material properties, and constraint conditions were the same as those described in Section 3.2.2.

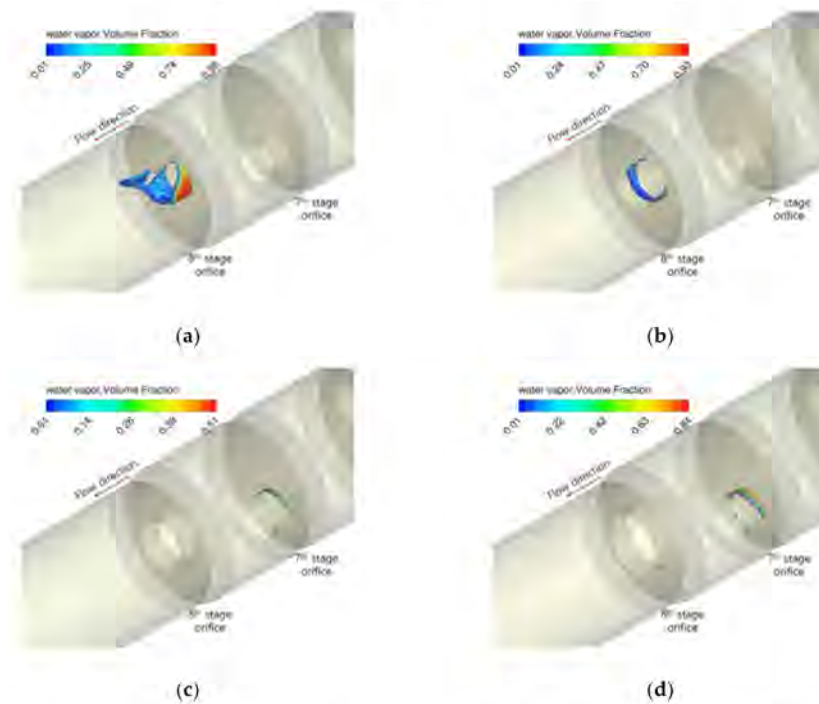
##### 4.3. The Computational Results

###### 4.3.1. Flow Analysis

Figure 19 shows the distribution of the vapor volume fraction in the second half of the multi-stage orifice depending on the size of the hole diameter ( $d_8$ ) in the eighth stage orifice. As the size of the hole diameter ( $d_8$ ) in the eighth stage orifice increased, the main cavitation region moved from the hole of the eighth stage orifice to that of the seventh stage orifice [16]. For  $d_8/d = 1.24$ , both the size of the cavitation region and the peak value of the vapor volume fraction were the smallest [16]. For  $d_8/d = 0.84$ , the cavitation region was extended to the downstream of the eighth stage orifice, and the maximum value of the vapor volume fraction was the largest [16]. In all cases, no cavitation region was formed upstream of the seventh stage orifice (i.e., from the inlet of the upstream connecting pipe to the inlet of the seventh stage orifice) [16].

On the other hand, in the case of the original multi-stage orifice ( $d_8/d = 1.0$ ) installed in the AFW pump recirculation line of the domestic NPP, a cavitation region was formed inside the hole of the eighth stage orifice under the design flow condition as shown in Figure 19b. Therefore, based on the simulation results of this study, it is necessary to review the adequacy of the multi-stage orifice design.

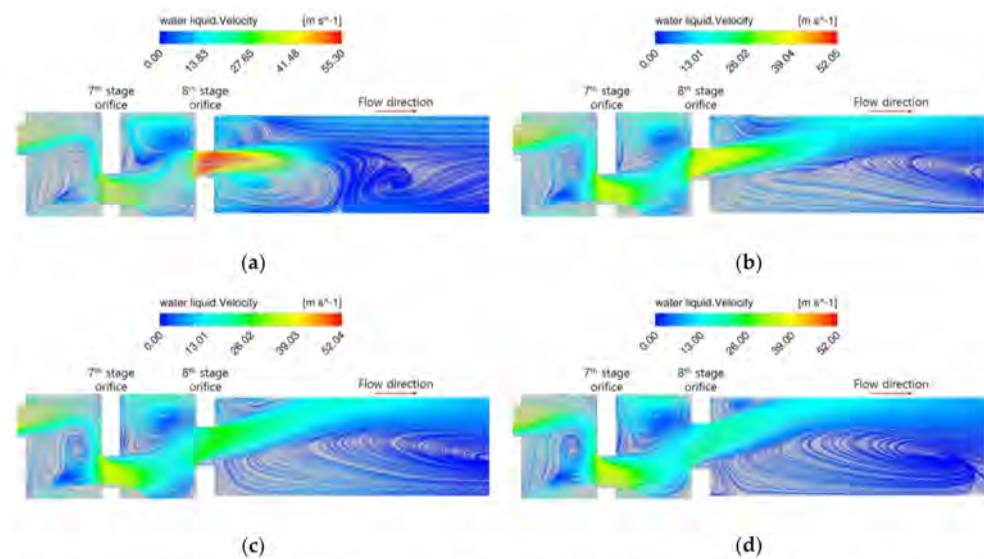




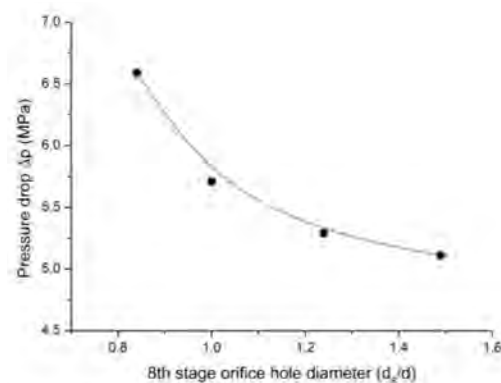
**Figure 19.** Iso-volume of vapor volume fraction depending on the size of the hole diameter ( $d_8$ ) in the eighth orifice stage: (a)  $d_8/d = 0.84$ ; (b)  $d_8/d = 1.0$  (original case); (c)  $d_8/d = 1.24$ ; and (d)  $d_8/d = 1.49$ .

Figure 20 shows the distribution of flow velocity and streamlines in the second half of a multi-stage orifice (for the symmetric  $y$ - $z$  plane) depending on the size of the hole diameter ( $d_8$ ) in the eighth orifice stage. In this study, only the hole diameter of the eighth stage orifice was changed and therefore the streamline pattern in the upstream of the eighth stage orifice was similar to each other [16]. On the other hand, since the location of the eighth stage orifice hole was higher than that of the seventh stage orifice hole, the flow passed through the eighth stage orifice hole upward [16]. The angle of this upward flow also increased as the size of the hole diameter in the eighth stage orifice increased [16]. As the size of the eighth stage orifice hole diameter was smaller, water (liquid phase) velocity passing through the eighth stage orifice hole was much faster [16]. Therefore, the peak value of the water (liquid phase) velocity for  $d_8/d = 0.84$  was found near the hole of the eighth stage orifice. For other  $d_8/d$  cases (for example,  $d_8/d = 1.0$ , 1.24, and 1.49), the maximum value of the water (liquid phase) velocity was shown near the hole entrance of the second stage orifice [16].

Figure 21 shows the pressure drop ( $\Delta p$ ) depending on the size of the hole diameter in the eighth stage orifice. The pressure drop ( $\Delta p$ ) is the difference in static pressure between the upstream and downstream cross-sections of the multi-stage orifice [16]. The corresponding cross-sections were located at 19 mm from the first and eighth stage orifice [16]. As shown in Figure 21, it was found that reducing the hole diameter in the eighth stage orifice resulted in increasing the pressure drop [16]. This trend in the static pressure drop can be also found in the experimental results of Wang et al. [3].



**Figure 20.** Distribution of flow velocity and streamlines in the second half of the multi-stage orifice (for the symmetric y-z plane) depending on the size of the hole diameter ( $d_8$ ) in the eighth orifice stage: (a)  $d_8/d = 0.84$ ; (b)  $d_8/d = 1.0$  (original case); (c)  $d_8/d = 1.24$ ; and (d)  $d_8/d = 1.49$ .



**Figure 21.** Pressure drop depending on the size of the hole diameter in the eighth stage orifice.

#### 4.3.2. Structural Analysis

Figure 22 and Table 8 show the predicted results of the stress intensity distribution in the multi-stage orifice and the connecting pipes depending on the hole diameter size of the eighth stage orifice under the design flow rate condition. For reference, numerical modeling for the structural analysis described in Section 4.2.2 was applied to ANSYS Mechanical. As the hole diameter of the eighth stage orifice decreased, the maximum value of the stress intensity increased. Similar to the analysis results in Section 3.2.2, because the flow entering into the multi-stage orifice experienced decompression in the process of passing through the orifice hole, it was judged that the maximum value of the stress intensity occurred in the connecting pipe upstream of the multi-stage orifice. However, it was confirmed that the hole diameter size of the eighth stage orifice did not significantly affect the stress intensity distribution in the multi-stage orifice and the connecting pipe. The predicted stress intensity distribution in the multi-stage orifice and the connecting pipe depending on the hole diameter size of the eighth orifice stage showed more margin for the allowable stress of 207 MPa than that for the operating flow rate ( $Q_{in} = 34.1, 37.0, 39.0,$  and  $41.5 \text{ m}^3/\text{h}$ ).

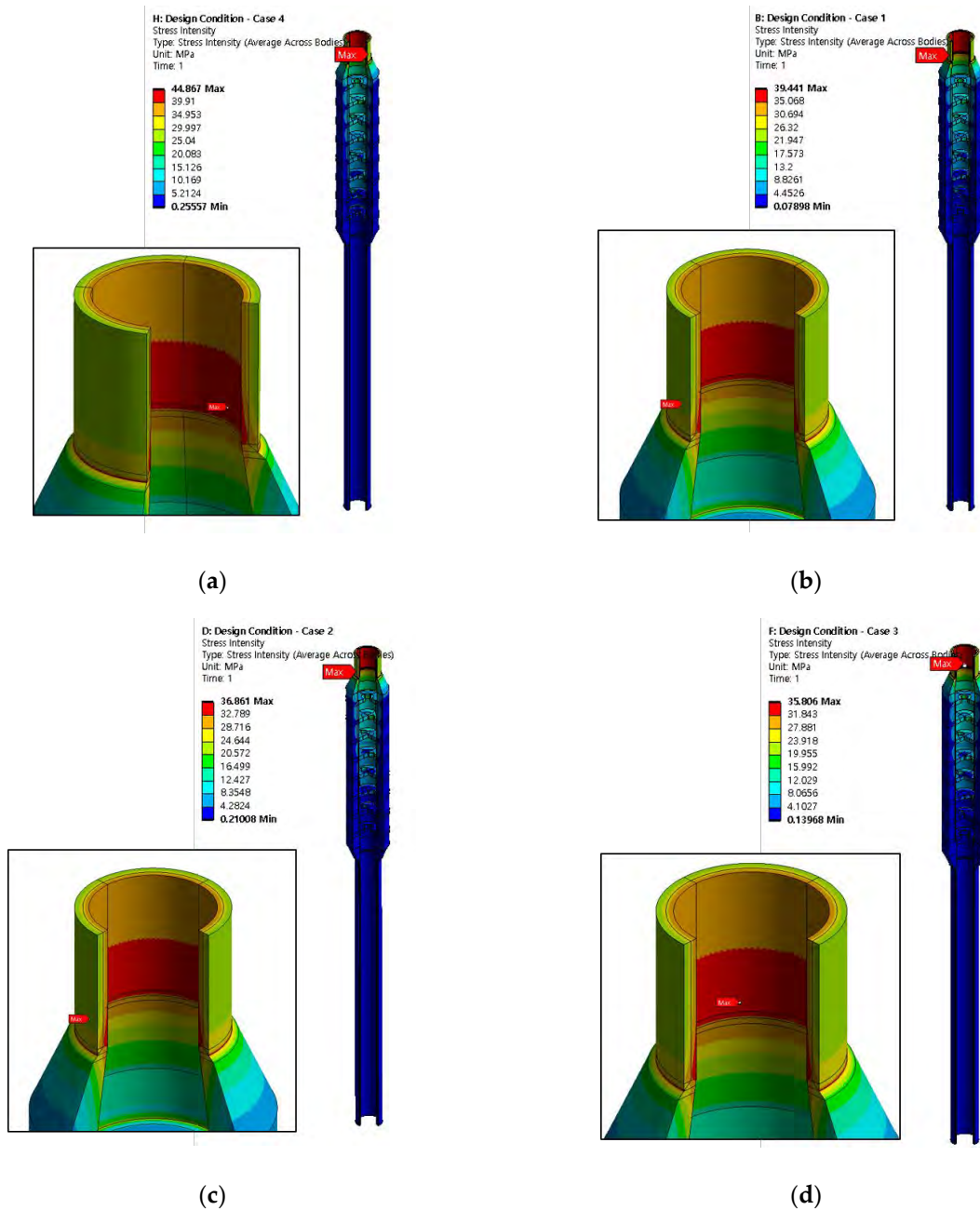


**Figure 22.** Distribution of stress intensity in the multi-stage orifice and the connecting pipes depending on the size of the hole diameter ( $d_8$ ) in the eighth orifice stage: (a)  $d_8/d = 0.84$ ; (b)  $d_8/d = 1.0$  (original case); (c)  $d_8/d = 1.24$ ; and (d)  $d_8/d = 1.49$ .

**Table 8.** The predicted results of stress components depending on the size of the hole diameter ( $d_8$ ) in the eighth orifice stage.

Case	Flowrate (m <sup>3</sup> /h)	Diameter Ratio ( $d_8/d$ )	Stress Intensity (MPa)	Membrane Stress (MPa)	Membrane + Bending Stress (MPa)	Allowable Stress (MPa)	Location of Maximum Stress
DS1	19.3	0.84	44.87	38.43	44.23	207	Upstream connecting pipe
DS2		1	39.44	33.77	38.88		
DS3		1.24	36.86	31.56	36.34		
DS4		1.49	35.81	30.65	35.3		

Table 9 shows the predicted deformation results for each direction in the multi-stage orifice and the connecting pipe depending on the hole diameter ( $d_8$ ) size of the eighth stage

orifice. In general, the smaller the hole diameter ( $d_8$ ) size of the eighth stage orifice, the greater the amount of deformation in each direction. At the same hole diameter ( $d_8$ ) size of the eighth stage orifice, the deformation size for each direction was in the order of axial > radial > hoop. For radial deformation, the maximum deformation value was shown in the upstream connecting pipe of the multi-stage orifice subjected to high stress. In the case of axial deformation, the maximum deformation value was indicated at the seventh or eighth stage orifice. For the deformation in the hoop direction, the maximum deformation value was shown either at the third stage orifice or in the downstream connecting pipe of the multi-stage orifice depending on the hole diameter ( $d_8$ ) size of the eighth stage orifice.

**Table 9.** The predicted results of deformation components depending on the size of the hole diameter ( $d_8$ ) in the eighth orifice stage.

Case	Flowrate (m <sup>3</sup> /h)	Diameter Ratio ( $d_8/d$ )	Max. Radial Deformation (mm)	Location of Max. Deformation	Max. Hoop Deformation (mm)	Location of Max. Deformation	Max. Axial Deformation (mm)	Location of Max. Deformation
DS1	19.3	0.84	0.0046	Upstream connecting pipe	0.0007	Downstream connecting pipe	0.0063	8th stage orifice
DS2		1	0.0041		0.0006		0.0049	
DS3		1.24	0.0038		0.0005	3rd stage orifice	0.0045	7th stage orifice
DS4		1.49	0.0037		0.0005		0.0044	

## 5. Conclusions

In this study, CFD simulation was performed for a six-stage orifice test facility to validate whether the numerical modeling available in ANSYS CFX R19.1 predicted reliably and accurately the complex flow inside the multi-stage orifice. In addition, to assess the adequacy of the changed operating flow rate proposed by the domestic NPP operator as a corrective measure for the flow leakage in the AFW pump recirculation line, the cavitation flow pattern in the multi-stage orifice and the connecting pipe depending on the operating flow rate was simulated. Additionally, using ANSYS Mechanical, the structural analysis was performed for the multi-stage orifice and the connecting pipe under the same operating flow rate condition used for the flow analysis, and the structural integrity was evaluated for the allowable stress. Finally, the effect of the change in the size of the hole diameter at the eighth-stage orifice on the pressure drop characteristics and flow patterns (including cavitation) under the design flow rate condition was evaluated. The main conclusions are as follows:

- For the six-stage orifice, selected as the benchmark analysis model, the difference in the static pressure drop between the orifice inlet and outlet depending on the operating flow rate was consistent within a maximum error of 5% compared to the measured data. Therefore, the numerical modeling applied in this study may be valid, and the calculation results may be judged to be reliable to a certain level. However, it is necessary to additionally provide detailed measurement data (velocity vector, vapor volume fraction, turbulence quantities, etc.) to validate the CFD software for complex flow patterns that can occur in the multi-stage orifice, including cavitation flow.
- As the operating flow rate increased, the cavitation region expanded, and through this, it was confirmed that the operating flow rate was a key factor to influence the cavitation behavior inside the multi-stage orifice. Therefore, the reduction of the operating flow rate proposed by the domestic NPP operator concerning the flow leakage in the AFW pump recirculation line is considered to be an appropriate corrective action. However, it was found that cavitation flow still happened even in the vicinity of the corrected operating flow rate, so it is necessary to conduct the operating time reduction of the AFW pump and periodic monitoring reinforcement (e.g., vibration measurement during the AFW pump operation, etc.) suggested as additional measures by the domestic NPP operator. Furthermore, it should be necessary to fundamentally review the adequacy of the multi-stage orifice design.

- As the operating flow rate increased, the maximum value of the stress intensity acting on the multi-stage orifice and the connecting pipe also increased but was predicted to be less than the allowable stress for the connecting pipe made of carbon steel in which the actual leakage occurred. Therefore, it is judged that the integrity of the multi-stage orifice and the connecting pipe can be maintained under the condition that there is no pipe thinning due to cavitation erosion.
- One of the important design considerations for the multi-stage orifice is to ensure that no cavitation occurs there. However, in the case of the original multi-stage orifice ( $d_8/d = 1.0$ ) installed in the AFW pump recirculation line of the domestic NPP, it was found that the cavitation region was formed inside the hole of the eighth stage orifice even when the corresponding flow rate was the reduced amount up to 54% compared to the operating flow rate. Therefore, it is necessary to review the appropriateness of the multi-stage orifice design.
- As the hole diameter size of the eighth stage orifice decreased, the maximum value of the stress intensity that occurred in the upstream connecting pipe of the multi-stage orifice increased. However, it was found that the change in the size of the hole diameter of the eighth stage orifice under the design flow rate condition did not significantly affect the stress intensity distribution in the multi-stage orifice and the connecting pipe.

**Author Contributions:** Conceptualization, G.L., J.B. and S.K.; methodology, G.L.; software, G.L.; validation, G.L.; formal analysis, G.L. and M.J.; investigation, G.L., J.B. and S.K.; resources, S.K. and J.B.; data curation, G.L.; writing—original draft preparation, G.L. and M.J.; writing—review and editing, G.L., M.J. and J.B.; visualization, G.L.; supervision, G.L.; project administration, G.L.; funding acquisition, G.L. All authors have read and agreed to the published version of the manuscript.

**Funding:** This work was supported by the Nuclear Safety Research Program through the Korea Foundation Of Nuclear Safety (KOFONS) using the financial resource granted by the Nuclear Safety and Security Commission (NSSC) of the Republic of Korea (No. 1805007).

**Acknowledgments:** This work was supported by the Supercomputing Center/Korea Institute of Science and Technology Information with supercomputing resources including technical support (project number: KSC-2019-CRE-0236). The author gratefully thanks Choi in the Central Research Center of Korea Hydro & Nuclear Power, Lee and Chang in the Tae Sung S&E for giving the valuable technical comments, and Lee in the Korea Institute of Nuclear Safety for providing the schematic diagram of the AFW system.

**Conflicts of Interest:** The authors declare no conflict of interest. The opinions expressed in this paper are those of the author and not necessarily those of the Korea Institute of Nuclear Safety (KINS). Any information presented here should not be interpreted as official KINS policy or guidance.

## References

1. Korea Hydro & Nuclear Power. *Comprehensive Action Plane for Leakage of the Welding Part, Reporting Material*; Korea Hydro & Nuclear Power: Gyeongju, Korea, 2018.
2. Lee, H.S.; Choi, M.H. Review of High Vibration of Multistage Orifice Piping by Cavitation. In Proceedings of the KSFM Annual Meeting, Pyeongchang, Korea, 3–5 July 2019; pp. 214–217.
3. Wang, H.; Xie, S.; Sai, Q.; Zhou, C.; Lin, H.; Chen, E. Experiment study on pressure drop of a multistage letdown orifice tube. *Nucl. Eng. Des.* **2013**, *265*, 633–638.
4. Bai, W.; Duan, Q.; Zhang, Z. Numerical investigation on cavitation within letdown orifice of PWR nuclear power plant. *Nucl. Eng. Des.* **2002**, *305*, 230–245. [[CrossRef](#)]
5. Niyogi, K.K.; Anton, S.; Majumdar, D.M. Prediction of Performance of Multi-stage Orifice Assembly using CFD Code. In Proceedings of the 26th International Conference on Nuclear Engineering, ICONE26-81186, London, UK, 22–26 July 2018.
6. Araoye, A.A.; Badr, H.M.; Ahmed, W.H. Investigation of flow through multi-stage restricting orifices. *Ann. Nucl. Energy* **2017**, *104*, 75–90. [[CrossRef](#)]
7. Lee, G.H.; Bae, J.H. Numerical study for the effect of diameter ratio magnitudes on the flow pattern around a flat orifice flowmeter. *J. Comput. Fluids Eng.* **2019**, *24*, 42–49. [[CrossRef](#)]
8. Menter, F. *CFD Best Practice Guidelines for CFD Code Validation for Reactor Safety Applications*; ECORA CONTRACT N°FIKS-CT-2001-00154; European Commission: Brussels, Belgium, 2002; p. 8.



9. ANSYS. Turbulence and Near-wall Modeling. In *ANSYS CFX-Solver Modeling Guide*; ANSYS: Canonsburg, PA, USA, 2018.
10. Lee, G.H.; Bae, J.H.; Kang, S.H. *Preliminary Assessment for the Welding Part Integrity of Multistage Orifice in the Auxiliary Feedwater System, NSTAR-20NS13-129*; Korea Foundation of Nuclear Safety: Seongnam, Korea, 2020.
11. Korea Hydro & Nuclear Power. Auxiliary Feedwater. In *The Final Safety Analysis Report*; Korea Hydro & Nuclear Power: Gyeongju, Korea, 2020.
12. Lee, G.H.; Bae, J.H. CFD Simulation of Cavitation Flow inside a Cavitating Venturi using ANSYS CFX. In Proceedings of the Transactions of the Korean Nuclear Society Spring Meeting, Jeju, Korea, 9–10 July 2020.
13. Lee, G.H.; Bae, J.H. Comparative study for the prediction of cavitating flow inside a square-edged orifice using different commercial CFD software. *E3S Web Conf.* **2019**, *128*, 1–3. [[CrossRef](#)]
14. Lee, G.H.; Bae, J.H. Assessment of Mesh Topology Effect on the Analysis Result of Cavitation Phenomenon inside an Orifice. In Proceedings of the KSCFE Spring Conference, Jeju, Korea, 3–5 July 2019.
15. ANSYS. Element Library. In *ANSYS Element Reference*; ANSYS: Canonsburg, PA, USA, 2020.
16. Lee, G.H.; Bae, J.H.; Kang, S.H. Numerical Study on the Flow Characteristics inside a Multi-stage Orifice depending on the Orifice Hole Diameter Sizes at the Design Condition. In Proceedings of the 31th International Symposium on Transport Phenomena, Honolulu, HI, USA, 13–16 October 2020.